Scavenging Potentially Heavy Metal/Metalloid/Nonmetal Atoms by Boron Nitride towards Soil Remediation: A Structural-Electromagnetic Analysis by DFT Study

Fatemeh Mollaamin*

Department of Biomedical Engineering, Faculty of Engineering and Architecture, Kastamonu University, Kastamonu, Turkey

Abstract: Soil pollution from toxic metals, metalloids, and nonmetals has become a major environmental problem around the world. Two main causes of this pollution are natural geogenic processes and human activities. While soils can acquire toxic metals from their original rock materials, most pollution comes from industries and farming. The presence of metals in soil can be detected by changes in chemical, biochemical, and microbial properties, as well as by plant reactions. The main goal of this study is to remove specific elements like Ba, As, Se, Co, Cu, and Mo from soil using a nanomaterial called boron nitride nanocage (B_5N_{10}). Scientists used materials modeling to demonstrate how the electromagnetic and thermodynamic properties of these elements change when they are trapped inside B_5N_{10}. The elements are held inside through chemisorption. The study examined how B_5N_{10} encapsulates Ba, As, Se, Co, Cu, and Mo, which aids in sensing metal ions in soil. B_5N_{10} was specifically designed to contain these elements. Researchers used the DFT method to analyze these cases. The study revealed that the covalent bonding in these complexes has similar energy levels and demonstrates boron and nitrogen in B_5N_{10} interact with the s states of barium and d states of "As, Se, Co, Cu, Mo" in the $[B_5(X)N_{10}]$ complexes. Nuclear magnetic resonance (NMR) analysis showed clear signals for "Ba, As, Se, Co, Cu, and Mo" during their trapping in B_5N_{10}. The findings indicate the order of adsorption selectivity for these elements by B_5N_{10} (as an atom sensor) is: Cu ≈ Co> Mo>>>As ≈ Se> Ba.

Keywords: Soil contamination, B_5N_{10}, Molecular modeling, Nanomaterial, DFT.

1. INTRODUCTION

Soil pollution stems from two main sources: natural processes and human activities. While soil can naturally accumulate toxic metals from the materials it is composed of, the majority of pollution is a consequence of the experiments in the industrial and agricultural laboratories. Signs of metal contamination in soil include alterations in its chemical, biological, and microbial composition, as well as changes in plant behavior. Although the total quantity of noxious metals in soil remains the most common method of assessing risk, some studies suggest that the amount of metal that plants absorb is a more accurate indicator. Common heavy metals found in polluted soil include cadmium, chromium, mercury, lead, copper, zinc, and arsenic. In recent times, heavy metal pollution has worsened due to industrial expansion, population growth, and intensified agricultural methods. These metals accumulate in water and soil, disrupting ecosystems. Furthermore, they travel through food chains, contaminating the food and water consumed by humans and animals, ultimately impacting their health [1-3].

Trace metals found in "soils/dust" can enter the skin through inhaling them, ingesting them, or absorbing them [4-7], as well as through the soil and crop system [8, 9]. Human-made sources of these metals include emissions from traffic, industry, and homes, as well as atmospheric deposits, mining activities, waste disposal, sewage, pesticides, and fertilizers [10-13]. Improper management of old or abandoned mines can result in more severe environmental problems than operating mines [14]. Consuming food grown in areas with metal contamination is a primary method through which people are exposed to these metals in mining regions [15-17].

Soil pollution in cities due to trace metals is a major concern for the public. To properly evaluate the risks, it is important to know the natural levels of these metals in city soils. For example, "molybdenum (Mo)" is a necessary trace element for humans, animals, and plants. A lack of Mo in soil is often found, especially when there is not enough phosphorus. However, Mo can also be harmful to soil and water systems and may cause serious problems for both the environment and people's health [18]. Another study examined the sources and distribution of arsenic, as well as its movement from microbes to soil and the various forms it can take [19]. Additionally, certain activities can elevate copper levels in the ground, which then insert the food chain and negatively impact both natural and managed environments [20].

Soil with high cobalt levels can be toxic to humans, plants, and animals. Newly, researchers have investigated the human-induced sources that contribute to increased "Co" in soil, as well as the

*Address correspondence to this author at the Department of Biomedical Engineering, Faculty of Engineering and Architecture, Kastamonu University, Kastamonu, Turkey; E-mail: fmollaamin@kastamonu.edu.tr

Received on 06-07-2026 Accepted on 10-08-2026 Published on 12-08-2026

E-ISSN: 2311-8741/26

different forms of cobalt present in soil and the parameters impacting its movement [21].

Soil pollution in cities due to trace metals is a major concern for the public. In order to fully comprehend the risks involved, it is essential to comprehend the typical levels of these metals found in city soils. A study was conducted to analyze the concentrations of 9 trace "metals - arsenic, barium, cadmium, cobalt, copper, nickel, lead, selenium, and zinc" - in 214 soil samples collected from various public and commercial areas in 6 cities of varying sizes in Florida [22].

Boron nitride nanomaterials are utilized for their unique features, such as being eco-friendly for absorbing pollutants, having a large surface area, strong chemical and mechanical properties, and acting as a semiconductor [23–26]. Boron nitride nanomaterials typically exhibit semiconducting behavior, making them a viable alternative to "CNT". The properties of "B" and "N" atoms, which are adjacent to "C" atoms, have made "BN" a popular topic for numerous investigations [27-29]. Recently, there have been numerous studies investigating how these materials can absorb chemical pollutants and serve as adsorbents for water purification [30-32]. Different shapes of boron nitride nano adsorbents are extensively studied due to their significant features, like a large surface area, flexible structures, strong chemical and mechanical properties, numerous structural defects, high reactivity, and numerous functional groups [33, 34].

In this study, B_5N_{10} has been utilized to encapsulate the "metal, metalloid, and nonmetal" atoms, such as "barium (Ba), arsenic (As), selenium (Se), cobalt (Co), copper (Cu), and molybdenum (Mo)". The physical and chemical interactions between these atoms and the boron and nitrogen in B_5N_{10} were analyzed.

2. NANOMATERIALS AND COMPUTATION PERSPECTIVE

2.1. Encapsulation in B_5N_{10}

The purpose of this research is to identify and encapsulate metal, metalloid, and nonmetal atoms from soil using B_5N_{10}. The goal is to extract harmful elements such as "Ba, As, Se, Co, Cu, and Mo" from soil contaminated with toxic substances. The soil contains a variety of atoms (metal, metalloid, nonmetal) and B_5N_{10} is introduced (as depicted in Figure **1**). B_5N_{10} was analyzed using computational methods based on density functional theory known as "CAM–B3LYP–D3".

"Metal, metalloid, and nonmetal" atoms were successfully positioned at the center of B_5N_{10}, forming complexes like $[B_5(Ba)N_{10}]$, $[B_5(As)N_{10}]$, $[B_5(Se)N_{10}]$, $[B_5(Co)N_{10}]$, $[B_5(Cu)N_{10}]$, and $[B_5(Mo)N_{10}]$ (as illustrated in Figure **1**).

The charge distribution of these complexes was determined using the Bader charge evaluation method [35]. Regardless of the element involved, the B_5N_{10} structure expands to accommodate these atoms.

2.2. Perspective of "Density functional theory (DFT)"

In a metallic solid, there are numerous ions and electrons that collectively form a complex system involving multiple particles. This article utilizes "density functional theory (DFT)" [36-39]. "Metals and metalloids" with calculated bandwidths have long been a significant topic of discussion when utilizing DFT. This paper presents first-principles calculations for elements such as "Ba, As, Se, Co, Cu, and Mo", which encompass metals, metalloids, and non-metals, employing "DFT" methods.

The "electronic density" in the "Kohn-Sham" equations significantly reduces the requirement for quantum computing when working with the Hamiltonian parameters [40,41]:

$$\hat{H}_s = -\sum_i^M \frac{1}{2}\nabla_i^2 + \sum_i^M v_s(\vec{r}_i) = \sum_i^M \hat{h}_s \;;\; \hat{h}_s = -\frac{1}{2}\nabla_i^2 + v_s(\vec{r}_i), \quad (1)$$

where *"M"* represents non-interacting electrons, and "v_s"is the external potential. Therefore, by evaluating ψ_i "(single-particle orbitals)", the parameter for the electronic density of non-interacting electrons will be:

$$\rho(\vec{r}) = \sum_i^M |\psi_i(\vec{r})|^2 \quad (2)$$

So, the total energy will be:

$$E[\rho] = \sum_i^M n_i \langle\psi_i \left| -\frac{1}{2}\nabla^2 + v_{ext}(\vec{r}) + \frac{1}{2}\int \frac{\rho(\vec{r}')}{|\vec{r}-\vec{r}'|}\,d\vec{r}' \right| \psi_i\rangle + E_{xc}[\rho] + \frac{1}{2}\sum_\beta^N \sum_{\alpha\neq\beta}^N \frac{Z_\alpha Z_\beta}{|\vec{R}_\alpha - \vec{R}_\beta|} \quad (3)$$

In addition, the "B3LYP (Becke, Lee, Yang, Parr)" method is a "hybrid functional" that utilizes a 3-parameter basis function in conjunction with the "LANL2DZ" basis set for "metals and metalloids" within the framework of density functional theory [42-47]. A new "hybrid exchange-correlation functional" called "CAM-B3LYP" was also introduced, which combines "B3LYP with long-range correction [48]. Furthermore, "DFT" functionals that incorporate "Grimme's D3 correction" have been discussed [49]. The method of "dispersion correction" was introduced into "Kohn-Sham" density functional theory "(DFT-D)" to enhance accuracy [50].

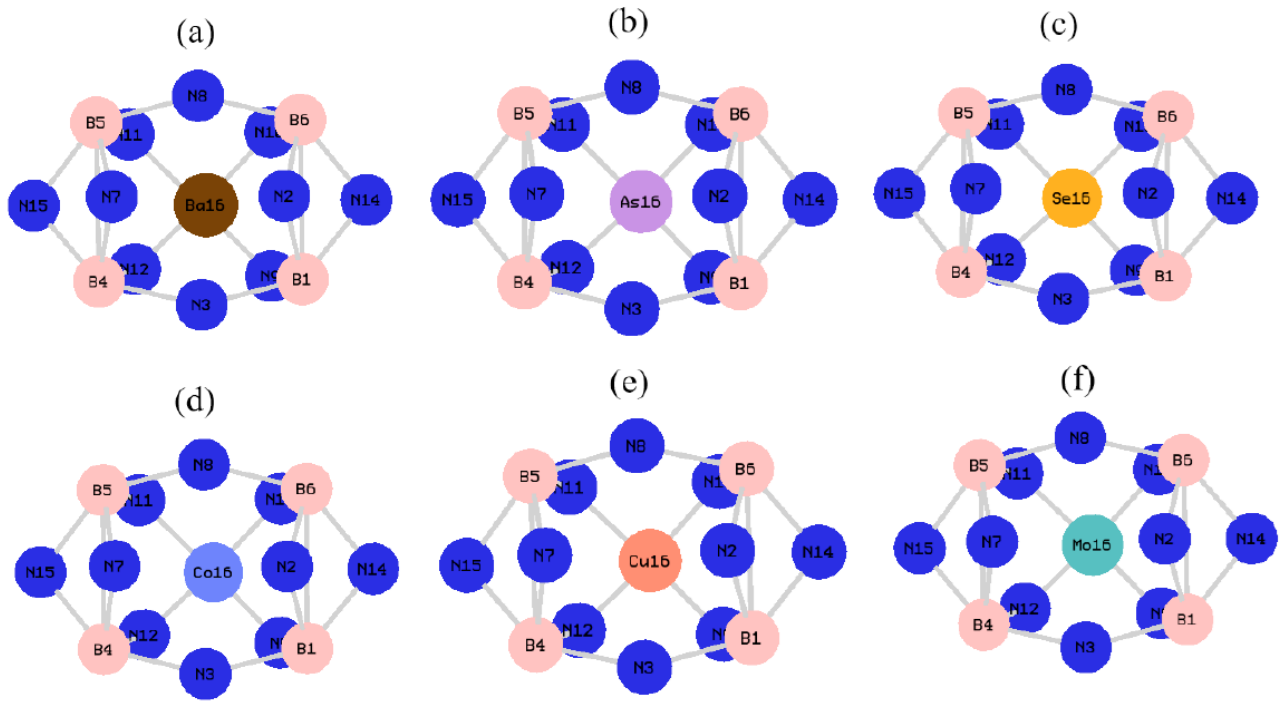

Figure 1: a) $[B_5(Ba)N_{10}]$, **b)** $[B_5(As)N_{10}]$, **c)** $[B_5(Se)N_{10}]$, **d)** $[B_5(Co)N_{10}]$, **e)** $[B_5(Cu)N_{10}]$, and **f)** $[B_5(Mo)N_{10}]$ complexes.

In this study, "DFT" calculations were conducted using the "Gaussian 16 revision C.01" software package [51]. The z-matrix structure was created to simulate the coordination of "metal, metalloid, and nonmetal" atoms such as "Ba, As, Se, Co, Cu, and Mo" within the soil, using B_5N_{10}. This was accomplished through Gauss View 6.1 [52] (Figure **1**).

The results will highlight the challenges that "DFT" methods face in accurately defining the bonding between "metal, metalloid, and nonmetal" elements with boron and nitrogen. The calculations used the basis sets of LANL2DZ for metals and 6–311+G(d,p) for other atoms with multiplicity of +1 and convergence on RMS density matrix=1.00D-08 and convergence on MAX density matrix=1.00D-06.

3. RESULTS AND DISCUSSIONS

B_5N_{10} has been designed to encapsulate the metal, metalloid, and nonmetal atoms such as "Ba, As, Se, Co, Cu, and Mo". The physical and chemical features of how these atoms interact with boron and nitrogen in B_5N_{10} have been studied and predicted.

3.1. PDOS towards Electronic Analysis

The electronic structure of how B_5N_{10} traps toxic elements such as "Ba, As, Se, Co, Cu, and Mo" have been studied by the "CAM–B3LYP–D3/6–311+G(d,p)" and "LANL2DZ" theoretical methods. Figure **2** (**a–f**) displays the "projected density of states (PDOS)" for $[B_5(X)N_{10}]$ when "Ba, As, Se, Co, Cu, and Mo" are encapsulated. The presence of energy levels from the s-orbitals of Ba, p-orbitals of "B and N" and d-orbitals of "As, Se, Co, Cu, and Mo" within the band gap of $[B_5(X)N_{10}]$ increases the system's reactivity. From the figure, it is evident that after trapping these atoms, there is a strong contribution from the d-orbitals in the unoccupied energy levels. This is clearly shown in the partial PDOS curves, which indicate that the s-states of Ba, p-states of B and N in B_5N_{10}, and d-orbitals of "As, Se, Co, Cu, and Mo" in $[B_5(X)N_{10}]$ all play a role in filling the "conduction band" (Figure **2a-f**). The unique adsorption behavior observed in $[B_5(X)N_{10}]$ is due to the strong interaction between the p-states of boron and nitrogen in B_5N_{10} and the s-states of barium and d-states of "As, Se, Co, Cu, and Mo" in the $[B_5(X)_{N10}]$ complexes.

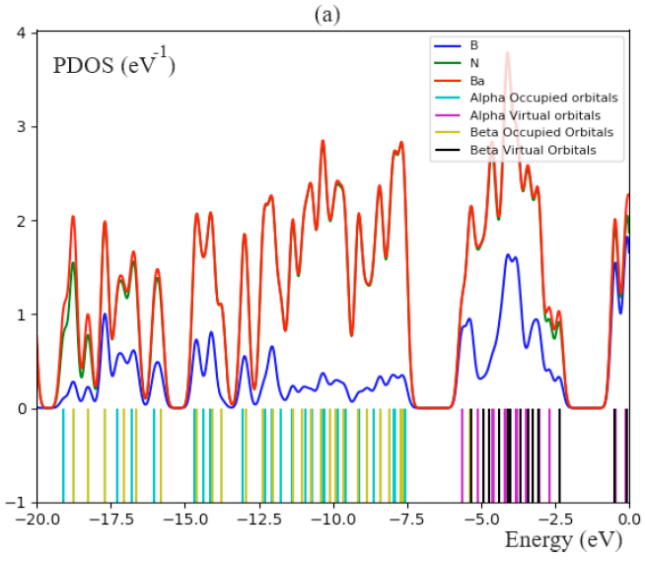

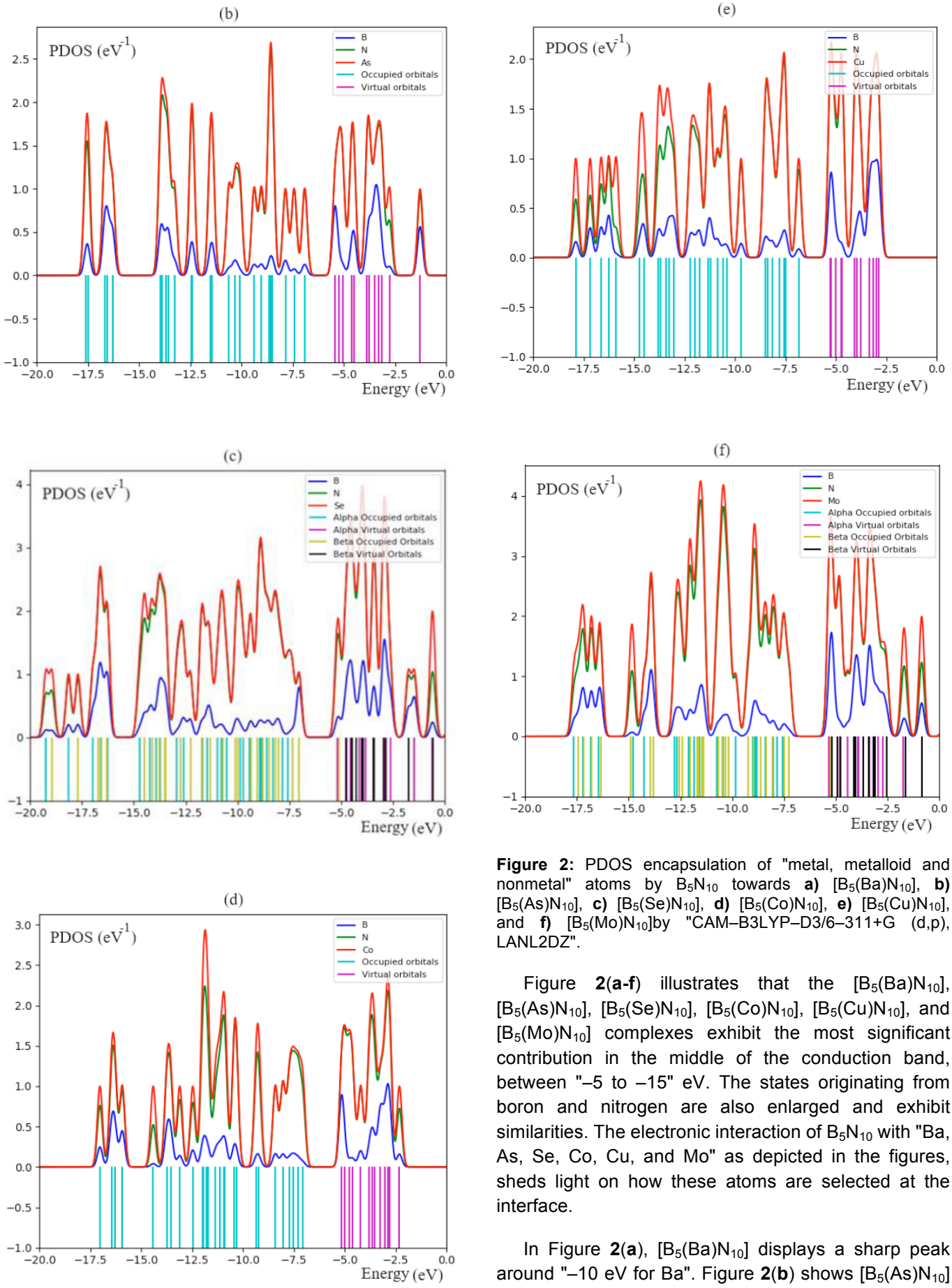

Figure 2: PDOS encapsulation of "metal, metalloid and nonmetal" atoms by B_5N_{10} towards **a)** [B_5(Ba)N_{10}], **b)** [B_5(As)N_{10}], **c)** [B_5(Se)N_{10}], **d)** [B_5(Co)N_{10}], **e)** [B_5(Cu)N_{10}], and **f)** [B_5(Mo)N_{10}]by "CAM–B3LYP–D3/6–311+G (d,p), LANL2DZ".

Figure **2**(**a-f**) illustrates that the [B_5(Ba)N_{10}], [B_5(As)N_{10}], [B_5(Se)N_{10}], [B_5(Co)N_{10}], [B_5(Cu)N_{10}], and [B_5(Mo)N_{10}] complexes exhibit the most significant contribution in the middle of the conduction band, between "–5 to –15" eV. The states originating from boron and nitrogen are also enlarged and exhibit similarities. The electronic interaction of B_5N_{10} with "Ba, As, Se, Co, Cu, and Mo" as depicted in the figures, sheds light on how these atoms are selected at the interface.

In Figure **2**(**a**), [B_5(Ba)N_{10}] displays a sharp peak around "–10 eV for Ba". Figure **2**(**b**) shows [B_5(As)N_{10}] with a sharp peak around "–8.5 eV for As", while Figure **2**(**c**) presents [B_5(Se)N_{10}] with a similar sharp peak

around "–8.5 eV for Se". $[B_5(Co)N_{10}]$ in Figure **2**(**d**) reveals a strong peak around "–12.5 eV for Co". The $[B_5(Cu)N_{10}]$ complex in Figure **2**(**e**) exhibits a noticeable sharp peak around "–7.5 eV for Cu". In Figure **2**(**f**), the $[B_5(Mo)N_{10}]$ complex displays two sharp peaks around "–10 and –12 eV for Mo". Based on the PDOS, the order of the atoms' uptake by B_5N_{10} is as follows: $[B_5(Mo)N_{10}] > [B_5(Co)N_{10}] > [B_5(Ba)N_{10}] > [B_5(As)N_{10}] \approx [B_5(Se)N_{10}] > [B_5(Cu)N_{10}]$. The presence of energy levels from the p-orbitals of B and N, and the d-orbitals of As, Se, Co, Cu, and Mo within the band gap of $[B_5(X)N_{10}]$ makes the system more reactive. From the figure, it is clear that after trapping transition metals, the d-orbitals contribute significantly to the unoccupied energy levels. This is shown by the partial PDOS curve, which indicates that the p-states of B and N atoms in BN, along with the d-orbitals of As, Se, Co, Cu, and Mo in $[B_5(X)N_{10}]$, interact with the conduction band.

3.2. Electric Potential Analysis

"Nuclear quadrupole resonance", or NQR, is a type of resonance related to "nuclear magnetic resonance (NMR)". It occurs when a spinning nucleus has an uneven distribution of electric charge. Any nucleus with a spin greater than 1 has both a "magnetic moment and an electric quadrupole moment". The quadrupole moment measures how much the positive charge inside the nucleus is spread out unevenly [53].

In this study, the "quantum mechanics of NQR" [54] at zero field, including the strengths of nuclear quadrupole moments, was explored. This was done by trapping atoms of barium (Ba), arsenic (As), selenium (Se), cobalt (Co), copper (Cu), and molybdenum (Mo) using B_5N_{10} [55-58]:

$$V(r) = V(0) + \left[\left(\frac{\partial V}{\partial x_i}\right)\Big|_0 . x_i\right] + \frac{1}{2}\left[\left(\frac{\partial^2 V}{\partial x_i x_j}\right)\Big|_0 . x_i x_j\right] + \ldots \quad (4)$$

$$U = -\frac{1}{2}\int_{\mathcal{D}} d^3\, r\, \rho_r \left[\left(\frac{\partial^2 V}{\partial x_i^2}\right)\Big|_0 . x_i^2\right] = -\frac{1}{2}\int_{\mathcal{D}} d^3\, r\, \rho_r \left[\left(\frac{\partial E_i}{\partial x_i}\right)\Big|_0 . x_i^2\right] = -\frac{1}{2}\left(\frac{\partial E_i}{\partial x_i}\right)\Big|_0 . \int_{\mathcal{D}} d^3\, r\, [\rho(r) . x_i^2] \quad (5)$$

$$\chi = {e^2 Q q_{zz}}/{h} \quad (6)$$

$$\eta = {q_{xx} - q_{yy}}/{q_{zz}} \quad (7)$$

The "electric field gradient (EFG)" at the nucleus location in "metal, metalloid, and nonmetal" atoms such as "Ba, As, Se, Co, Cu, and Mo" are determined by the arrangement of "valence electrons" around the nucleus. This arrangement is influenced by the presence of these atoms in compounds with a B_5N_{10} structure. The EFG leads to specific nuclear quadrupole resonance (NQR) frequencies that are observed only in $[B_5(X)N_{10}]$ complexes, where X represents "Ba, As, Se, Co, Cu, or Mo" (as shown in Tables **1** and **2**).

Table1: "Electric potential (a.u.)" and "Bader charge (coulomb)" through "NQR" computation for $[B_5(Ba)N_{10}]$, $[B_5(As)N_{10}]$, and $[B_5(Se)N_{10}]$ complexes

$[B_5(Ba)N_{10}]$			$[B_5(As)N_{10}]$			$[B_5(Se)N_{10}]$		
Atom	**Charge**	**Electric potential**	**Atom**	**Charge**	**Electric potential**	**Atom**	**Charge**	**Electric potential**
B(1)	0.173	–11.197	B(1)	0.168	–11.204	B(1)	0.165	–11.221
N(2)	–0.237	–18.305	N(2)	–0.138	–18.315	N(2)	–0.121	–18.301
N(3)	–0.429	–18.334	N(3)	–0.310	–18.311	N(3)	–0.191	–18.312
B(4)	0.228	–11.205	B(4)	0.236	–11.204	B(4)	0.226	–11.220
B(5)	0.229	–11.210	B(5)	0.247	–11.204	B(5)	0.231	–11.222
B(6)	0.200	–11.200	B(6)	0.190	–11.204	B(6)	0.181	–11.224
N(7)	–0.219	–18.307	N(7)	–0.115	–18.314	N(7)	–0.133	–18.306
N(8)	–0.405	–18.339	N(8)	–0.273	–18.303	N(8)	–0.158	–18.305
N(9)	–0.385	–18.349	N(9)	–0.329	–18.309	N(9)	–0.282	–18.335
N(10)	–0.370	–18.344	N(10)	–0.278	–18.296	N(10)	–0.241	–18.325
N(11)	–0.339	–18.328	N(11)	–0.278	–18.297	N(11)	–0.230	–18.317
N(12)	–0.469	–18.366	N(12)	–0.383	–18.310	N(12)	–0.348	–18.326
B(13)	–0.058	–11.172	B(13)	–0.174	–11.160	B(13)	–0.193	–11.193
N(14)	–0.117	–18.278	N(14)	–0.160	–18.297	N(14)	–0.116	–18.292
N(15)	–0.094	–18.289	N(15)	–0.147	–18.284	N(15)	–0.104	–18.280
Ba(16)	2.294	–4.9859	As(16)	1.748	–2.228	Se(16)	1.316	–2.925

Table 2: "Electric potential (a.u.)" and "Bader charge (coulomb)" through "NQR" computation for $[B_5(Co)N_{10}]$, $[B_5(Cu)N_{10}]$, and $[B_5(Mo)N_{10}]$complexes

$[B_5(Co)N_{10}]$			$[B_5(Cu)N_{10}]$			$[B_5(Mo)N_{10}]$		
Atom	**Charge**	**Electric potential**	**Atom**	**Charge**	**Electric potential**	**Atom**	**Charge**	**Electric potential**
B(1)	0.226	–11.215	B(1)	0.227	–11.209	B(1)	0.195	–11.219
N(2)	–0.046	–18.285	N(2)	–0.039	–18.287	N(2)	–0.080	–18.293
N(3)	–0.125	–18.289	N(3)	–0.128	–18.297	N(3)	–0.160	–18.306
B(4)	0.235	–11.215	B(4)	0.229	–11.210	B(4)	0.218	–11.212
B(5)	0.249	–11.213	B(5)	0.252	–11.215	B(5)	0.239	–11.210
B(6)	0.218	–11.214	B(6)	0.217	–11.214	B(6)	0.222	–11.211
N(7)	–0.065	–18.305	N(7)	–0.050	–18.290	N(7)	–0.063	–18.294
N(8)	–0.133	–18.284	N(8)	–0.135	–18.306	N(8)	–0.169	–18.305
N(9)	–0.042	–18.295	N(9)	–0.018	–18.286	N(9)	–0.179	–18.317
N(10)	–0.055	–18.291	N(10)	–0.044	–18.291	N(10)	–0.164	–18.308
N(11)	–0.055	–18.287	N(11)	–0.038	–18.292	N(11)	–0.171	–18.303
N(12)	–0.064	–18.288	N(12)	–0.065	–18.289	N(12)	–0.177	–18.313
B(13)	0.330	–11.215	B(13)	0.268	–11.203	B(13)	0.447	–11.220
N(14)	–0.111	–18.299	N(14)	–0.110	–18.287	N(14)	–0.051	–18.286
N(15)	–0.142	–18.290	N(15)	–0.135	–18.278	N(15)	–0.093	–18.290
Co(16)	–0.417	–21.075	Cu(16)	–0.430	–26.063	Mo(16)	–0.012	–10.727

In this study, the electric potential for these complexes was calculated using the "Bader charge" method, including $[B_5(Ba)N_{10}]$, $[B_5(As)N_{10}]$, $[B_5(Se)N_{10}]$, $[B_5(Co)N_{10}]$, $[B_5(Cu)N_{10}]$, and $[B_5(Mo)N_{10}]$ (Tables **1** and **2**).

In Figure **3** (**a**-**f**), the electric potential fluctuations related to the Bader charge for "toxic metal, metalloid, and nonmetal atoms" such as "Ba, As, Se, Co, Cu, and Mo", which are encapsulated by the B_5N_{10}, have been evaluated.

In Figure **3** (**a-f**), it is evident that B_5N_{10} encapsulates fluctuations of "Ba, As, Se, Co, Cu, and Mo", aiding in the detection of toxic metals, metalloids, and nonmetals in polluted soil. The graph of B_5N_{10} displays a curve caused by these toxic elements. The most significant changes in electric potential were observed when "metal, metalloid, and nonmetal atoms" were trapped by B_5N_{10}, indicating that these elements gain electrons with the assistance of "boron and nitrogen atoms" in B_5N_{10}. The order of these interactions, based on the R^2 correlation coefficient, is: $[B_5(Mo)N_{10}] > [B_5(Cu)N_{10}] > [B_5(Co)N_{10}] > [B_5(As)N_{10}] \approx [B_5(Se)N_{10}] > [B_5(Ba)N_{10}]$ (Figure **3a-f**).

The sharpest changes in electric potential with $R_2 \approx 0.99$ are seen when metal, metalloid, and nonmetal atoms are trapped by B_5N_{10}, showing that electrons from these elements are encapsulated with help from boron and nitrogen atoms in B_5N_{10}. Adding certain transition metals increases the magnetization levels, especially. Calculations using spin-polarized DFT band structures show clear spin differences caused by doping, which backs up our theoretical results on the doped B_5N_{10} samples.

3.3. "Nuclear Magnetic Resonance (NMR)"

The study of "NMR" in high-performance materials and other systems with correlated electrons has helped improve understanding of conventional super-conductors, as well as "d-band transition metals, alloys, and intermetallic" compounds. "Magnetic field gradients" make it possible to identify specific spatial positions within a model. The resonance frequencies of most atoms are clearly different from each other, making "NMR" a method that can distinguish between elements. The interaction of spins with their local surroundings leads to changes in the spectrum that reveal the local structure and chemical state. Therefore, the NMR spectrum of B_5N_{10} could show how it can encapsulate the "metal, metalloid, and nonmetal" atoms like "Ba, As, Se, Co, Cu, and Mo". This might indicate the potential of B_5N_{10} for detecting and removing these harmful elements from polluted soil, as

(a)

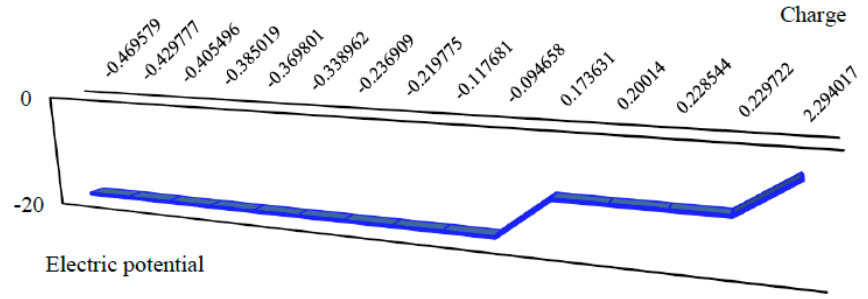
Charge
-0.469579
-0.429777
-0.405496
-0.385019
-0.369801
-0.338962
-0.236909
-0.219775
-0.117681
-0.094658
0.173631
0.20014
0.228544
0.229722
2.294017
0
-20
Electric potential

(b)

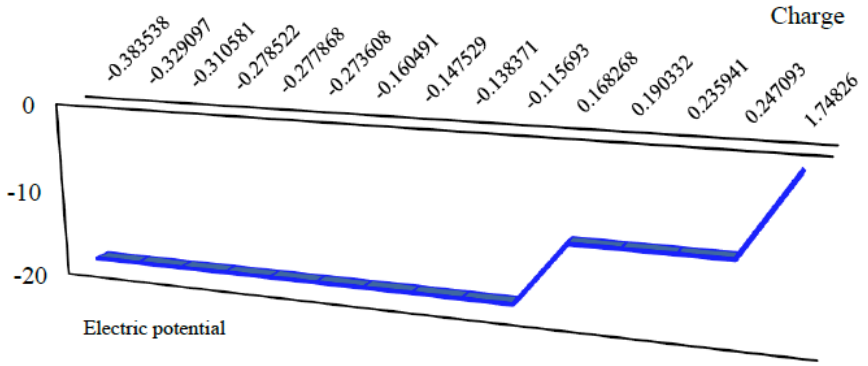
Charge
-0.383538
-0.329097
-0.310581
-0.278522
-0.277868
-0.273608
-0.160491
-0.147529
-0.138371
-0.115693
0.168268
0.190332
0.235941
0.247093
1.74826
0
-10
-20
Electric potential

(c)

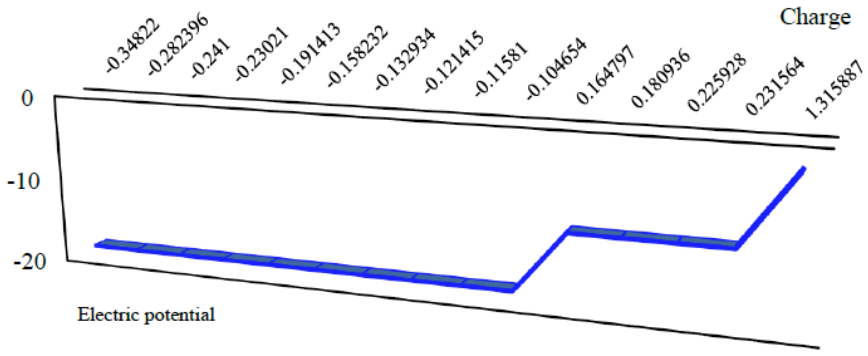
Charge
-0.34822
-0.282396
-0.241
-0.23021
-0.191413
-0.158232
-0.132934
-0.121415
-0.11581
-0.104654
0.164797
0.180936
0.225928
0.231564
1.315887
0
-10
-20
Electric potential

(d)

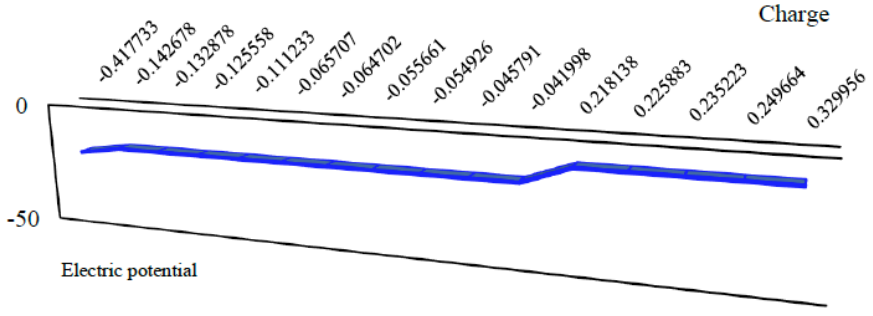
Charge
-0.417733
-0.142678
-0.132878
-0.125558
-0.111233
-0.065707
-0.064702
-0.055661
-0.054926
-0.045791
-0.041998
0.218138
0.225883
0.235223
0.249664
0.329956
0
-50
Electric potential

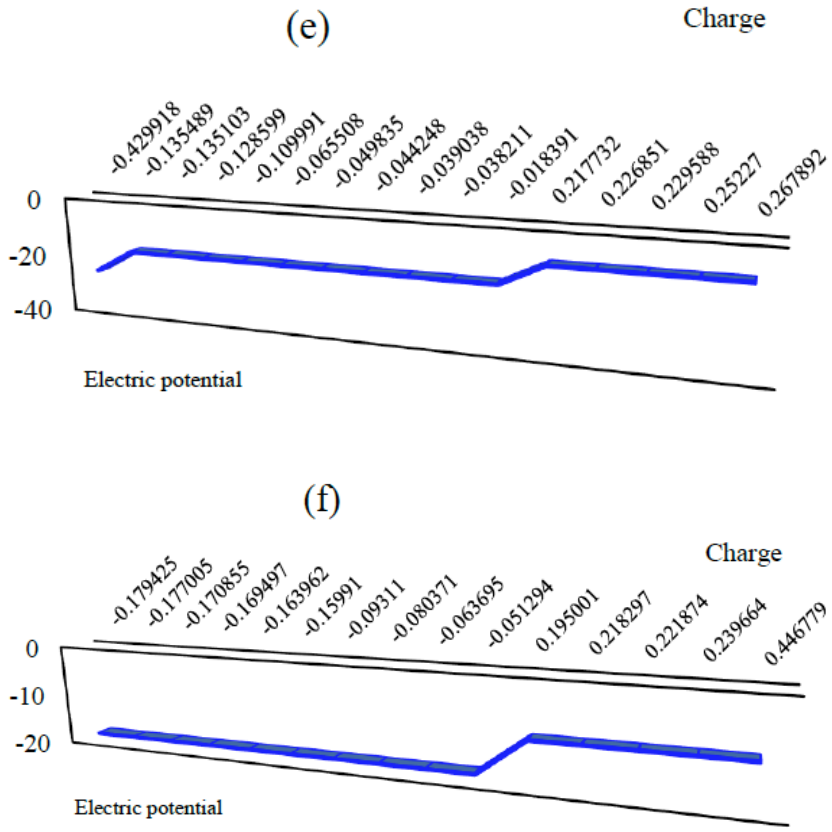

Figure 3: "Electric potential (a.u.)" versus "Bader charge (coulomb)" through "NQR" calculation for complexes of **a)** $[B_5(Ba)N_{10}]$, **b)** $[B_5(As)N_{10}]$, **c)** $[B_5(Se)N_{10}]$, **d)** $[B_5(Co)N_{10}]$, **e)** $[B_5(Cu)N_{10}]$, and **f)** $[B_5(Mo)N_{10}]$.

Table 3: NMR shielding (isotropic/anisotropic) tensors for $[B_5(Ba)N_{10}]$, $[B_5(As)N_{10}]$, and $[B_5(Se)N_{10}]$ complexes

$[B_5(Ba)N_{10}]$			$[B_5(As)N_{10}]$			$[B_5(Se)N_{10}]$		
Atom	**Isotropy**	**Anisotropy**	**Atom**	**Isotropy**	**Anisotropy**	**Atom**	**Isotropy**	**Anisotropy**
B(1)	76.442	84.033	B(1)	82.012	80.015	B(1)	125.781	73.750
N(2)	228.657	335.420	N(2)	338.384	432.032	N(2)	360.726	941.314
N(3)	404.564	662.908	N(3)	187.741	774.417	N(3)	506.852	655.424
B(4)	75.310	91.245	B(4)	76.653	83.777	B(4)	113.160	106.285
B(5)	81.517	72.188	B(5)	78.319	78.218	B(5)	106.858	68.773
B(6)	73.941	87.167	B(6)	87.197	74.203	B(6)	127.683	76.793
N(7)	257.352	463.125	N(7)	553.312	682.031	N(7)	263.729	614.075
N(8)	522.900	493.102	N(8)	68.082	539.582	N(8)	543.826	727.584
N(9)	407.998	522.586	N(9)	177.024	603.977	N(9)	152.759	526.414
N(10)	548.953	973.672	N(10)	182.188	725.789	N(10)	179.371	679.603
N(11)	645.374	1226.565	N(11)	179.027	952.587	N(11)	227.317	581.252
N(12)	305.057	522.151	N(12)	270.343	482.003	N(12)	98.907	603.909
B(13)	93.995	111.410	B(13)	105.420	95.759	B(13)	129.833	66.214
N(14)	331.435	737.220	N(14)	532.748	1213.659	N(14)	305.365	585.678
N(15)	393.606	831.536	N(15)	565.785	1222.441	N(15)	282.190	765.749
Ba(16)	62.871	8.819	As(16)	32.193	5.952	Se(16)	32.894	9.582

well as for measuring "isotropic" and "anisotropic chemical shielding" effects [59-61]:

$$\sigma_{iso} = (\sigma_{11} + \sigma_{22} + \sigma_{33})/3 \quad (8) \quad ; \quad \sigma_{aniso} = \sigma_{33} - (\sigma_{22} + \sigma_{11})/2 \quad (9)$$

Table 4: NMR shielding (isotropic/anisotropic) tensors for selected atoms of $[B_5(Co)N_{10}]$, $[B_5(Cu)N_{10}]$, and $[B_5(Mo)N_{10}]$ complexes using CAM–B3LYP–D3/6–311+G(d,p), LANL2DZ calculations

$[B_5(Co)N_{10}]$			$[B_5(Cu)N_{10}]$			$[B_5(Mo)N_{10}]$		
Atom	**Isotropy**	**Anisotropy**	**Atom**	**Isotropy**	**Anisotropy**	**Atom**	**Isotropy**	**Anisotropy**
B(1)	95.016	86.277	B(1)	24.138	182.358	B(1)	89.090	67.251
N(2)	281.213	515.692	N(2)	1230.134	1717.794	N(2)	9.242	257.905
N(3)	324.101	892.551	N(3)	7928.231	14686.887	N(3)	248.759	498.866
B(4)	104.739	59.786	B(4)	22.408	204.418	B(4)	91.094	72.787
B(5)	99.010	71.971	B(5)	67.041	67.304	B(5)	80.179	69.368
B(6)	91.963	84.796	B(6)	92.603	86.945	B(6)	78.285	78.533
N(7)	419.148	586.431	N(7)	900.174	2259.314	N(7)	80.141	209.403
N(8)	396.235	1132.961	N(8)	256.307	3595.664	N(8)	348.368	801.455
N(9)	331.110	542.547	N(9)	927.114	7561.802	N(9)	511.839	667.325
N(10)	445.186	811.937	N(10)	2393.922	3515.727	N(10)	450.884	664.125
N(11)	333.804	828.184	N(11)	1732.711	2923.788	N(11)	320.625	491.593
N(12)	56.286	417.825	N(12)	105.166	2377.665	N(12)	193.021	493.859
B(13)	59.524	60.928	B(13)	79.376	83.443	B(13)	15.091	217.576
N(14)	573.121	1964.542	N(14)	126.851	3820.801	N(14)	392.800	945.997
N(15)	118.615	945.992	N(15)	275.161	3332.103	N(15)	374.205	986.530
Co(16)	4862.426	4932.587	Cu(16)	12057.026	16337.955	Mo(16)	167.813	116.213

The "NMR" values for "isotropic shielding (σ_{iso})" and "anisotropic shielding tensor (σ_{aniso})" of "Ba, As, Se, Co, Cu, and Mo", which are encapsulated in B_5N_{10}, were calculated to form the complexes $[B_5(Ba)N_{10}]$, $[B_5(As)N_{10}]$, [B5(Se)N10], $[B_5(Co)N_{10}]$, $[B_5(Cu)N_{10}]$, and $[B_5(Mo)N_{10}]$. These computations were done using the "Gaussian 16 revision C.01 program" package (Tables **3** & **4**).

Tables **3** and **4** display the NMR values for "metal, metalloid, and nonmetal elements" such as "Ba, As, Se, Co, Cu, and Mo" that are enclosed within B_5N_{10}. When these elements are encapsulated by B_5N_{10}, they induce a spin polarization effect on the "(Ba, As, Se, Co, Cu, Mo)"-encapsulated B_5N_{10}. The chemical shift anisotropy increases when these atoms are trapped by B_5N_{10}, particularly near nitrogen atoms at positions "N(2), N(3), N(7), N(8), N(9), N(10), N(11), N(12), N(14), and N(15)" (Tables **3** and **4**). The weak signal intensity observed near the parallel edge of the nanocage may be attributed to the "non-spherical distribution" of these structures resulting from boron binding. It is evident that trapping "Ba, As, Se, Co, Cu, and Mo" in B_5N_{10} can enhance the stability of the nanocluster and elevate the magnetic properties of the clusters (Tables **3** and **4**). Figure **4**(**a-f**) illustrates that the "shielding factor" for both "boron and nitrogen" is similar, but a noticeable difference arises when "Ba, As, Se, Co, Cu, and Mo" are encapsulated by B_5N_{10} through their interactions with boron and nitrogen atoms.

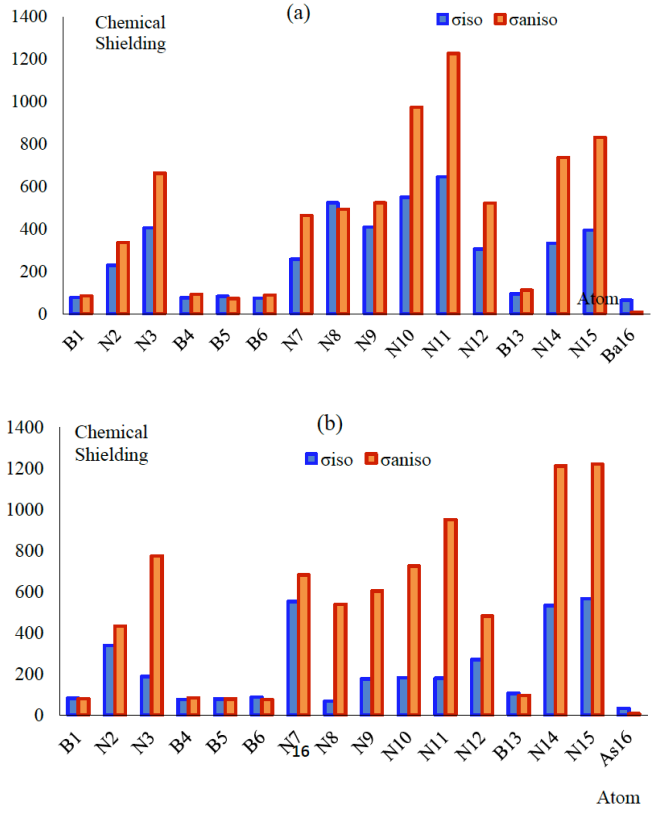

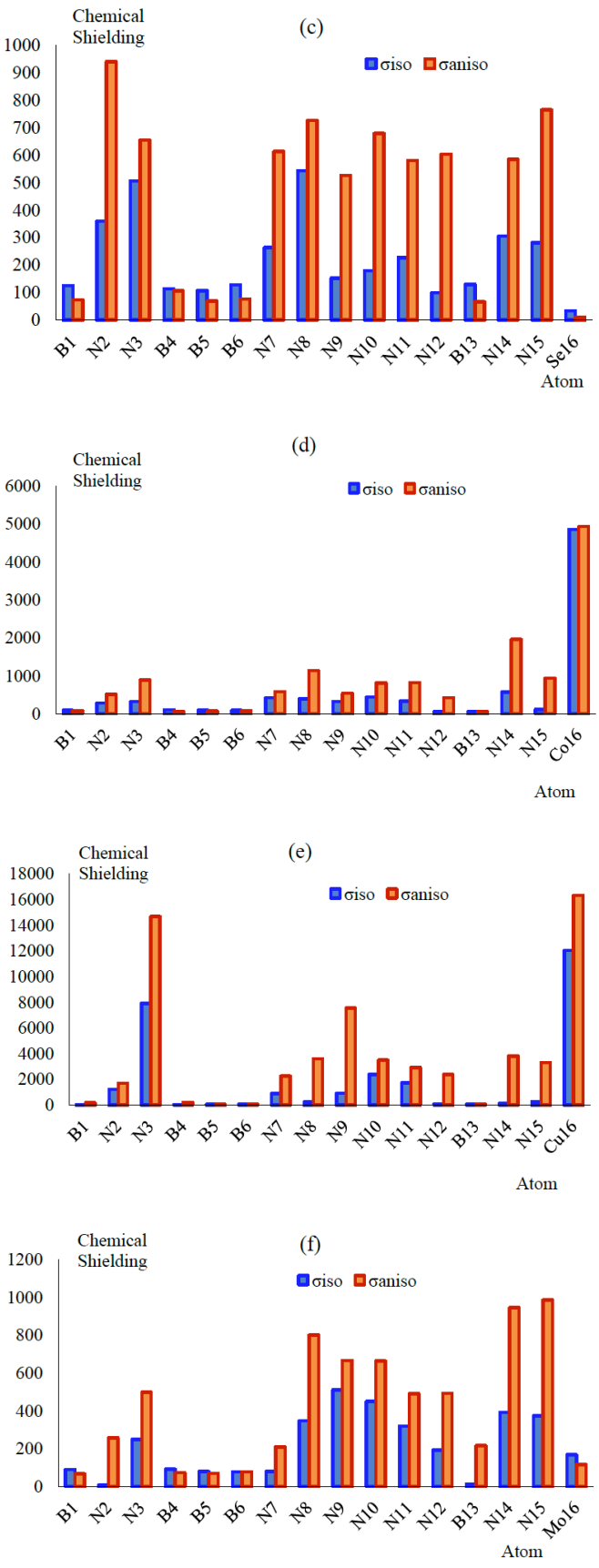

Figure 4: "NMR" spectra for **a)** $[B_5(Ba)N_{10}]$, **b)** $[B_5(As)N_{10}]$, **c)** $[B_5(Se)N_{10}]$, **d)** $[B_5(Co)N_{10}]$, **e)** $[B_5(Cu)N_{10}]$, and **f)** $[B_5(Mo)N_{10}]$.

In Figure **4** (**a-f**), the toxic elements "Ba, As, Se, Co, Cu, and Mo" in the complexes $[B_5(Ba)N_{10}]$ (Figure **4a**), $[B_5(As)N_{10}]$ (Figure **4b**), $[B_5(Se)N_{10}]$ (Figure **4c**), $[B_5(Co)N_{10}]$ (Figure **4d**), $[B_5(Cu)N_{10}]$ (Figure **4e**), and $[B_5(Mo)N_{10}]$ (Figure **4f**) exhibit changes in "chemical shielding" during atom encapsulation. Figure **4** (**a-f**) illustrates the "chemical shielding" between "boron/nitrogen" in B_5N_{10} and "metal, metalloid, and nonmetal atoms".

This indicates that the ability of B_5N_{10} to accept electrons for the encapsulated toxic atoms follows the order Cu ≈ Co> Mo >>>As ≈Se > Ba, suggesting the strength of the covalent bonds between "boron/nitrogen" and these elements during atom encapsulation. The curves for the "metal, metalloid, and nonmetal elements" "Ba, As, Se, Co, Cu, and Mo" demonstrate how these elements are trapped in B_5N_{10}.

This proves the strength of the covalent bond between boron/nitrogen and these elements, which helps in atom encapsulation. The curves of "Ba, As, Se, Co, Cu, and Mo", as metal, metalloid, and nonmetal elements, show how these elements are trapped in B_5N_{10}during atom detection and removal from soil.

3.4. Thermochemical Analysis

The study examined the ability of B_5N_{10} to trap "metal, metalloid, and nonmetal elements" such as "Ba, As, Se, Co, Cu, and Mo" using thermochemical parameters. $[B_5(Ba)N_{10}]$, $[B_5(As)N_{10}]$, $[B_5(Se)N_{10}]$, $[B_5(Co)N_{10}]$, $[B_5(Cu)N_{10}]$, and $[B_5(Mo)N_{10}]$ complexes were analyzed utilizing thermochemical data observed in Table **5**. It was indicates that B_5N_{10}, with its capability to encapsulate these elements, could serve as a more effective tool for sensing and detecting them in soil.

Table **5** shows how "metal, metalloid, and nonmetal elements" such as "Ba, As, Se, Co, Cu, and Mo" can be encapsulated by B_5N_{10}. The process of trapping these elements in B_5N_{10} is supported by the values of ΔG^o_{ads}:

$$\Delta G^o_{ads} = \Delta G^o_{[B5(X)N10]} - \left(\Delta G^o_{X-encapsulated} + \Delta G^o_{B5N10}\right); \quad X= Ba, As, Se, Co, Cu, Mo \tag{10}$$

It has been shown that the interaction between the adsorbates, which include metals, metalloids, and nonmetals acting as electron acceptors, and the adsorbent B_5N_{10} acting as an electron donor, depends on the size of the atoms involved. This leads to the selectivity of these elements by B5N10, which functions as an atom sensor, following the order: Cu > Co > Mo > Ba > Se ≈ As, as indicated in Table **5**.

4. CONCLUSION

B_5N_{10} can be utilized to extract "metal, metalloid, and nonmetal elements" from soil through "electrostatic

Table 5: The thermochemical characters of stability energy, thermal enthalpy, Gibbs free energy, entropy and dipole moments (D/debye) for $[B_5(Ba)N_{10}]$, $[B_5(As)N_{10}]$, $[B_5(Se)N_{10}]$, $[B_5(Co)N_{10}]$, $[B_5(Cu)N_{10}]$, and $[B_5(Mo)N_{10}]$ complexes

Compound	D (debye)	$\Delta E^{\circ}\times10^{-3}$ (kcal/mol)	$\Delta H^{\circ}\times10^{-3}$ (kcal/mol)	$\Delta G^{\circ}\times10^{-3}$ (kcal/mol)	S° (cal/K.mol)
$[B_5(Ba)N_{10}]$	0.7328	–435.016	–435.016	–435.041	85.684
$[B_5(As)N_{10}]$	0.7092	–423.975	–423.975	–424.001	89.715
$[B_5(Se)N_{10}]$	0.4392	–425.815	–425.814	–425.842	92.311
$[B_5(Co)N_{10}]$	0.1927	–511.393	–511.393	–511.421	93.652
$[B_5(Cu)N_{10}]$	0.5245	–543.331	–543.330	–543.359	96.138
$[B_5(Mo)N_{10}]$	0.5314	–462.582	–462.581	–462.608	89.861

interactions" between these elements and B_5N_{10}. The thermochemistry and electromagnetic properties of "Ba, As, Se, Co, Cu, and Mo" adsorbed onto B_5N_{10} have been examined using the DFT method. The findings indicate that "Ba, As, Se, Co, Cu, and Mo" trapped in B_5N_{10} are highly stable, with the most stable position being at the center of the B_5N_{10} structure. The process of capturing these elements in B_5N_{10} occurs through chemisorption, and after adsorption, B5N10 demonstrates a strong affinity for them. The work function of B_5N_{10} has been shown to significantly enhance its ability to adsorb "metal, metalloid, and nonmetal elements", with the best performance observed in the Cu> Co> Mo> Ba> Se ≈ As– adsorbed B_5N_{10} system.

CONFLICTS OF INTEREST

The author declared no conflict of interest.

REFERENCES

[1] HE, Z., Shentu, J., Yang, X., Baligar, V.C., Zhang, T. & Stoffella, P.J. Heavy Metal Contamination of Soils: Sources, Indicators, and Assessment, Journal of Environmental Indicators, 9: 17-18, 2015. https://doi.org/10.3390/app2030584

[2] Rahman, S.H.; Khanam, D.; Adyel, T.M.; Islam, M.S.; Ahsan, M.A.; Akbor, M.A. Assessment of Heavy Metal Contamination of Agricultural Soil around Dhaka Export Processing Zone (DEPZ), Bangladesh: Implication of Seasonal Variation and Indices. Appl. Sci. 2012, 2, 584-601.

[3] Thuy, H., Tobschall, H. & An, P. Distribution of heavy metals in urban soils - a case study of Danang-Hoian Area (Vietnam). Environmental Geology 39, 603-610 (2000). https://doi.org/10.1007/s002540050472

[4] De Miguel, E.; De Grado, M.J.; Llamas, J.F.; Martín-Dorado, A.; Mazadiego, L.F. The overlooked contribution of compost application to the trace elements in playgrounds in Madrid (Spain). Sci. Total Environ. 1998, 215, 113-122. https://doi.org/10.1016/S0048-9697(98)00112-0

[5] Madrid, L.; Díaz-Barrientos, F.; Madrid, F. Distribution of heavy metal contents of urban soils in parks of Seville. Chemosphere 2002, 49, 1301-1308. https://doi.org/10.1016/S0045-6535(02)00530-1

[6] Meza-Montenegro, M.M.; Gandolfi, A.J.; Santana-Alcántar, M.E.; Klimecki, W.T.; Aquilar-Apodaca, M.G.; Del Río-Salas, R.; De la O-Villanueva, M.; Gómez-Alvarez, A.; Mendivil-Quijada, H.; Valencia, M.; et al. Metals in residential soils and cumulative risk assessment in Yaqui and Mayo agricultural valleys, northern Mexico. Sci. Total Environ. 2012, 433, 472-481. https://doi.org/10.1016/j.scitotenv.2012.06.083

[7] Sun, G.Y.; Li, Z.G.; Bi, X.Y.; Chen, Y.P.; Lu, S.F.; Yuan, X. Distribution, sources and health risk assessment of mercury in kindergarten dust. Atmos. Environ. 2013, 73, 169-176. https://doi.org/10.1016/j.atmosenv.2013.03.017

[8] Liu, W.X.; Shen, L.F.; Liu, J.W.; Wang, Y.W.; Li, S.R. Uptake of toxic heavy metals by rice (Oryza sativa L.) cultivated in the agricultural soils near Zhengzhou City. People's Republic of China. Bull. Environ. Contam. Toxicol. 2007, 79, 209-213. https://doi.org/10.1007/s00128-007-9164-0

[9] Sun, G.Y.; Chen, Y.P.; Bi, X.Y.; Yang, W.; Chen, X.S.; Zhang, B.; Cui, Y.J. Geochemical assessment of agricultural soil: A case study in Songnen-Plain (Northeastern China). Catena 2013, 111, 56-63. https://doi.org/10.1016/j.catena.2013.06.026

[10] Sezgin, N.; Ozcan, H.K.; Demir, G.; Nemlioglu, S.; Bayat, C. Determination of heavy metal concentrations in street dusts in Istanbul E-5 highway. Environ. Int. 2003, 29, 979-985. https://doi.org/10.1016/S0160-4120(03)00075-8

[11] Montagne, D.; Cornu, S.; Bourennane, H.N.; Baize, D.; Ratié, C.; King, D. Effect of agricultural practices on trace-element distribution in soil. Commun. Soil Sci. Plant Anal. 2007, 38, 473-491. https://doi.org/10.1080/00103620601174411

[12] Li, Y.; Gou, X.; Wang, G.; Zhang, Q.; Su, Q.; Xiao, G. Heavy metal contamination and source in arid agricultural soils in central Gansu province, China. J. Environ. Sci. 2008, 20, 607-612. https://doi.org/10.1016/S1001-0742(08)62101-4

[13] Morton-Bermea, O.; Hernández-Alvarez, E.; González-Hernández, G.; Romero, F.; Lozano, R.; Beramendi-Orosco, L.E. Assessment of heavy metal pollution in urban topsoils from the metropolitan area of Mexico City. J. Geochem. Explor. 2009, 101, 218-224. https://doi.org/10.1016/j.gexplo.2008.07.002

[14] Ji, K.; Kim, J.K.; Lee, M.J.; Park, S.Y.; Kwon, H.J.; Cheong, H.K.; Jang, J.Y.; Kim, D.S.; Yu, S.; Kim, Y.W.; et al. Assessment of exposure to heavy metals and health risks among residents near abandoned metal mines in Goseong, Korea. Environ. Pollut. 2013, 178, 322-328. https://doi.org/10.1016/j.envpol.2013.03.031

[15] Liu, H.; Probst, A.; Liao, B. Metal contamination of soils and crops affected by the Chenzhou lead/zinc mine spill (Hunan, China). Sci. Total Environ. 2005, 339, 153-166. https://doi.org/10.1016/j.scitotenv.2004.07.030

[16] Kim, S.; Cho, Y.M.; Choi, S.H.; Kim, H.J.; Choi, J. The effect of exposure factors on the concentration of heavy metals in residents near abandoned metal mines. J. Prev. Med. Public Health 2011, 44, 41-47. https://doi.org/10.3961/jpmph.2011.44.1.41

[17] Kachenko, A.G.; Singh, B. Heavy metals contamination in vegetables grown in urban and metal smelter contaminated

sites in Australia. Water Air Soil Pollut. 2006, 169, 101-123. https://doi.org/10.1007/s11270-006-2027-1

[18] G.V. Motuzova, T.M. Minkina, E.A. Karpova, N.U. Barsova, S.S. Mandzhieva, Soil contamination with heavy metals as a potential and real risk to the environment, Journal of Geochemical Exploration, 144, Part B, 241-246, 2014. https://doi.org/10.1016/j.gexplo.2014.01.026

[19] Al-Makishah, N.H., Taleb, M.A. & Barakat, M.A. Arsenic bioaccumulation in arsenic-contaminated soil: a review. Chem. Pap. 74, 2743-2757 (2020). https://doi.org/10.1007/s11696-020-01122-4

[20] Giovana Poggere, Amanda Gasparin, Julierme Zimmer Barbosa, George Wellington Melo, Rodrigo Studart Corrêa, Antonio Carlos Vargas Motta, Soil contamination by copper: Sources, ecological risks, and mitigation strategies in Brazil, Journal of Trace Elements and Minerals, 4, 100059, 2023. https://doi.org/10.1016/j.jtemin.2023.100059

[21] Miao Jiang, Kun Wang, Yipeng Wang, Qingliang Zhao, Weiye Wang, Technologies for the cobalt-contaminated soil remediation: A review, Science of The Total Environment, 813, 151908, 2022. https://doi.org/10.1016/j.scitotenv.2021.151908

[22] Evandro B. da Silva, Peng Gao, Min Xu, Dongxing Guan, Xianjin Tang, Lena Q. Ma, Background concentrations of trace metals As, Ba, Cd, Co, Cu, Ni, Pb, Se, and Zn in 214 Florida urban soils: Different cities and land uses, Environmental Pollution, 264, 114737,2010. https://doi.org/10.1016/j.envpol.2020.114737

[23] D. Gonzalez-Ortiz, C. Salameh, M. Bechelany, P. Miele, Nanostructured boron nitride-based materials: synthesis and applications. Mater. Today Adv., 8 (2020), p. 100107. https://doi.org/10.1016/j.mtadv.2020.100107

[24] N.S. Mishra, P. Saravanan, A review on the synergistic features of hexagonal boron nitride (white graphene) as adsorbent-photo active nanomaterial. ChemistrySelect, 3 (28) (2018), pp. 8023-8034. https://doi.org/10.1002/slct.201801524

[25] Q.H. Weng, X.B. Wang, X. Wang, Y. Bando, D. Golberg, Functionalized hexagonal boron nitride nanomaterials: emerging properties and applications. Chem. Soc. Rev., 45 (14) (2016), 3989-4012. https://doi.org/10.1039/C5CS00869G

[26] Alma Delia Ocotitla Muñoz, Alejandro Escobedo-Morales, Ehsan Skakerzadeh, Ernesto Chigo Anota, Effect of homonuclear boron bonds in the adsorption of DNA nucleobases on boron nitride nanosheets. J. Mol. Liquids, 322, 114951, 2021. https://doi.org/10.1016/j.molliq.2020.114951

[27] Shtansky, D.V.; Matveev, A.T.; Permyakova, E.S.; Leybo, D.V.; Konopatsky, A.S.; Sorokin, P.B. Recent Progress in Fabrication and Application of BN Nanostructures and BN-Based Nanohybrids. Nanomaterials 2022, 12, 2810. https://doi.org/10.3390/nano12162810

[28] Yang, Y.; Peng, Y.; Saleem, M.F.; Chen, Z.; Sun, W. Hexagonal Boron Nitride on III-V Compounds: A Review of the Synthesis and Applications. Materials 2022, 15, 4396. https://doi.org/10.3390/ma15134396

[29] Davies, A.; Albar, J.D.; Summerfield, A.; Thomas, J.C.; Cheng, T.S.; Korolkov, V.V.; Stapleton, E.; Wrigley, J.; Goodey, N.L.; Mellor, C.J.; et al. Lattice-Matched Epitaxial Graphene Grown on Boron Nitride. Nano Lett. 2018, 18, 498-504. https://doi.org/10.1021/acs.nanolett.7b04453

[30] R.S. Bangari, V.K. Yadav, J.K. Singh, N. Sinha, Fe3O4-functionalized boron nitride nanosheets as novel adsorbents for removal of arsenic(III) from contaminated water. ACS Omega, 5 (18) (2020), pp. 10301-10314. https://doi.org/10.1021/acsomega.9b04295

[31] Y.H. Chao, J. Zhang, H.P. Li, P.W. Wu, X.W. Li, H.H. Chang, J. He, H.F. Wu, H.M. Li, W.S. Zhu, Synthesis of boron nitride nanosheets with N-defects for efficient tetracycline antibiotics adsorptive removal. Chem. Eng. J., 387 (2020), 124138. https://doi.org/10.1016/j.cej.2020.124138

[32] Mollaamin, F., Mohammadi, S., Khalaj, Z. et al. Computational Modelling of Boron Nitride Nanosheet for Detecting and Trapping of Water Contaminant. Russ. J. Phys. Chem. B 18, 67-82 (2024). https://doi.org/10.1134/S1990793124010330

[33] Mollaamin, F. Features of parametric point nuclear magnetic resonance of metals implantation on boron nitride nanotube by density functional theory/electron paramagnetic resonance. Journal of Computational and Theoretical Nanoscience, 2014, 11(11), 2393-2398. https://doi.org/10.1166/jctn.2014.3653

[34] Y. Guo, R.X. Wang, P.F. Wang, L. Rao, C. Wang, Developing a novel layered boron nitride-carbon nitride composite with high efficiency and selectivity to remove protonated dyes from water. ACS Sustain. Chem., 7 (6) (2019), 5727-5741. https://doi.org/10.1021/acssuschemeng.8b05150

[35] G Henkelman, A Arnaldsson, and H Jónsson, “A fast and robust algorithm for Bader decomposition of charge density,” Computational Materials Science 36(3), 354-360 (2006). https://doi.org/10.1016/j.commatsci.2005.04.010

[36] Blöchl, P.E. Projector augmented-wave method. Phys. Rev. B 1994, 50, 17953-17979. https://doi.org/10.1103/PhysRevB.50.17953

[37] Mollaamin, F., Monajjemi, M. Graphene-based resistant sensor decorated with Mn, Co, Cu for nitric oxide detection: Langmuir adsorption & DFT method. Sensor Review, 2023, 43(4), 266-279. https://doi.org/10.1108/SR-03-2023-0040

[38] Mollaamin, F.; Monajjemi, M. Graphene Embedded with Transition Metals for Capturing Carbon Dioxide: Gas Detection Study Using QM Methods. Clean Technol. 2023, 5, 403-417. https://doi.org/10.3390/cleantechnol5010020

[39] Mollaamin, F.; Monajjemi, M. Doping of Graphene Nanostructure with Iron, Nickel and Zinc as Selective Detector for the Toxic Gas Removal: A Density Functional Theory Study. C 2023, 9 (1), 20. https://doi.org/10.3390/c9010020

[40] Hohenberg, P.; Kohn, W. Inhomogeneous Electron Gas. Phys. Rev. B, 1964, 136, B864-B871. https://doi.org/10.1103/PhysRev.136.B864

[41] Kohn, W.; Sham, L. J. Self-Consistent Equations Including Exchange and Correlation Effects. Phys. Rev., 1965, 140, A1133- A1138. https://doi.org/10.1103/PhysRev.140.A1133

[42] Becke AD (1993) Density-functional thermochemistry. III. The role of exact exchange. J Chem Phys 98:5648-5652. https://doi.org/10.1063/1.464913

[43] Lee C, Yang W, Parr RG (1988) Development of the Colle-Salvetti correlation-energy formula into a functional of the electron density. Phys Rev B 37:785-789. https://doi.org/10.1103/PhysRevB.37.785

[44] K. Kim; K. D. Jordan (1994). "Comparison of Density Functional and MP2 Calculations on the Water Monomer and Dimer". J. Phys. Chem. 98 (40): 10089-10094. https://doi.org/10.1021/j100091a024

[45] P. J. Stephens; F. J. Devlin; C. F. Chabalowski; M. J. Frisch (1994). "Ab Initio Calculation of Vibrational Absorption and Circular Dichroism Spectra Using Density Functional Force Fields". J. Phys. Chem. 98 (45): 11623-11627. https://doi.org/10.1021/j100096a001

[46] C. J. Cramer (2004). "Essentials of Computational Chemistry: Theories and Models, 2nd Edition Wiley". Wiley.com. Retrieved 2021-06-24.

[47] S. H. Vosko; L. Wilk; M. Nusair (1980). "Accurate spin-dependent electron liquid correlation energies for local spin density calculations: a critical analysis". Can. J. Phys. 58 (8): 1200-1211. Bibcode: 1980CaJPh..58.1200V. https://doi.org/10.1139/p80-159

[48] Takeshi Yanai a, David P Tew b, Nicholas C Handy, A new hybrid exchange-correlation functional using the Coulomb-attenuating method (CAM-B3LYP), Chemical

Physics Letters, 393, (1-3), 51-57, 2004. https://doi.org/10.1016/j.cplett.2004.06.011

[49] Stefan Grimme, Jens Antony, Stephan Ehrlich, Helge Krieg, A consistent and accurate ab initio parametrization of density functional dispersion correction (DFT-D) for the 94 elements H-Pu, J Chem Phys. 2010 Apr 21; 132(15): 154104. https://doi.org/10.1063/1.3382344

[50] Stefan Grimme, Stephan Ehrlich, Lars Goerigk, Effect of the damping function in dispersion corrected density functional theory. J Comput Chem. 2011; 32(7): 1456-65. https://doi.org/10.1002/jcc.21759

[51] Frisch, M. J.; Trucks, G. W.; Schlegel, H. B.; Scuseria, G. E.; Robb, M. A.; et al. Gaussian 16, Revision C.01, Gaussian, Inc., Wallingford CT, 2016.

[52] GaussView, Version 6.06.16, Dennington, Roy; Keith, Todd A.; Millam, John M. Semichem Inc., Shawnee Mission, KS, 2016.

[53] Ahluwalia, V.K. (2023). Nuclear Quadrupole Resonance (NQR) Spectroscopy. In: Instrumental Methods of Chemical Analysis. Springer, Cham. https://doi.org/10.1007/978-3-031-38355-7_30

[54] Bruno Herreros and Gerard S. Harbison, Nuclear Quadrupole Resonance, Characterization of Materials, 1st ed., Vol. 2, pp. 775-792, by, University of Nebraska, Lincoln, Nebraska; Published online: October 15, 2002;

[55] Smith, J. A. S. (January 1971). "Nuclear Quadrupole Resonance Spectroscopy". Journal of Chemical Education. 48: 39-41. https://doi.org/10.1021/ed048p39

[56] Appendix K: Nuclear quadrupole resonance, by Allen N. Garroway, Naval Research Laboratory. In Jacqueline MacDonald, J. R. Lockwood: Alternatives for Landmine Detection. Report MR-1608, Rand Corporation, 2003.

[57] O. Kh. Poleshchuck, E.L. Kalinna, J. N. Latosinska, J. Koput, Journal of Molecular Structure (Theochem) 547 (2001) 233-243. https://doi.org/10.1016/S0166-1280(01)00636-4

[58] Young, Hugh A.; Freedman, Roger D. (2012). Sears and Zemansky's University Physics with Modern Physics (13th ed.). Boston: Addison-Wesley. p. 754.

[59] Walstedt, R.E. (2018). Introduction to NMR Studies of Metals, Metallic Compounds, and Superconductors. In: The NMR Probe of High-Tc Materials and Correlated Electron Systems. Springer Tracts in Modern Physics, vol 276. Springer, Berlin, Heidelberg. https://doi.org/10.1007/978-3-662-55582-8

[60] Sohail, U.; Ullah, F.; Binti Zainal Arfan, N.H.; Abdul Hamid, M.H.S.; Mahmood, T.; Sheikh, N.S.; Ayub, K. Transition Metal Sensing with Nitrogenated Holey Graphene: A First-Principles Investigation. Molecules 2023, 28, 4060. https://doi.org/10.3390/molecules28104060

[61] M.T. Caccamo, G. Sabatino, A. Bennardo and S. Magazù, Infrared spectroscopy analysis of montmorillonite thermal effects. 2020 IOP Conf. Ser.: Mater. Sci. Eng. 777, 012002. https://doi.org/10.1088/1757-899X/777/1/012002

https://doi.org/10.12974/2311-8741.2026.14.04